Systems/Circuits

Neuropeptide Modulation Increases Dendritic Electrical Spread to Restore Neuronal Activity Disrupted by Temperature

Margaret L. DeMaegd and [®]Wolfgang Stein

School of Biological Sciences, Ilinois State University, Normal, Illinois 61790

Peptide neuromodulation has been implicated to shield neuronal activity from acute temperature changes that can otherwise lead to loss of motor control or failure of vital behaviors. However, the cellular actions neuropeptides elicit to support temperature-robust activity remain unknown. Here, we find that peptide neuromodulation restores rhythmic bursting in temperature-compromised central pattern generator (CPG) neurons by counteracting membrane shunt and increasing dendritic electrical spread. We show that acutely rising temperatures reduced spike generation and interrupted ongoing rhythmic motor activity in the crustacean gastric mill CPG. Neuronal release and extrinsic application of Cancer borealis tachykininrelated peptide Ia (CabTRP Ia), a substance-P-related peptide, restored rhythmic activity. Warming led to a significant decrease in membrane resistance and a shunting of the dendritic signals in the main gastric mill CPG neuron. Using a combination of fluorescent calcium imaging and electrophysiology, we observed that postsynaptic potentials and antidromic action potentials propagated less far within the dendritic neuropil as the system warmed. In the presence of CabTRP Ia, membrane shunt decreased and both postsynaptic potentials and antidromic action potentials propagated farther. At elevated temperatures, CabTRP Ia restored dendritic electrical spread or extended it beyond that at cold temperatures. Selective introduction of the CabTRP Ia conductance using a dynamic clamp demonstrated that the CabTRP Ia voltage-dependent conductance was sufficient to restore rhythmic bursting. Our findings demonstrate that a substance-P-related neuropeptide can boost dendritic electrical spread to maintain neuronal activity when perturbed and reveals key neurophysiological components of neuropeptide actions that support pattern generation in temperature-compromised conditions.

Key words: membrane shunt; neuromodulation; neuropil; pattern generation; peptide; stomatogastric

Significance Statement

Changes in body temperature can have detrimental consequences for the well-being of an organism. Temperature-dependent changes in neuronal activity can be especially dangerous if they affect vital behaviors. Understanding how temperature changes disrupt neuronal activity and identifying how to ameliorate such effects is critically important. Our study of a crustacean circuit shows that warming disrupts rhythmic neuronal activity by increasing membrane shunt and reducing dendritic electrical spread in a key circuit neuron. Through the ionic conductance activated by it, substance-P-related peptide modulation restored electrical spread and counteracted the detrimental temperature effects on rhythmic activity. Because neuropeptides are commonly implicated in sustaining neuronal activity during perturbation, our results provide a promising mechanism to support temperature-robust activity.

Received Jan. 16, 2021; revised June 17, 2021; accepted June 22, 2021.

Author contributions: M.L.D. and W.S. designed research; M.L.D. and W.S. performed research; M.L.D. analyzed data; and M.L.D. and W.S. wrote the paper.

This work was supported by grants from the National Science Foundation (NSF IOS 1755098) to W.S. and the 2021 Cheung, Brown, Phi Sigma Award for Student Publications and the Illinois State University Dissertation Award to M.L.D.

The authors declare no competing financial interests.

Correspondence should be addressed to Wolfgang Stein at wstein@neurobiologie.de. https://doi.org/10.1523/JNEUROSCI.0101-21.2021

Copyright © 2021 the authors

Introduction

Passive electrical propagation in dendrites is necessary to support summation required for action potential (AP) initiation. Because dendrites rarely support active AP propagation, changes in biophysical membrane properties, such as ionic conductance levels, can significantly alter electrical spread (Hoffman et al., 1997; Short et al., 2017; Otopalik et al., 2019). Acute temperature changes are known to alter active and passive biophysical properties but rarely do so linearly or equally across properties, which can disrupt neuronal activity (Collins and Rojas, 1982; Hille, 2001; Cao and Oertel, 2005). For example, hyperthermia is

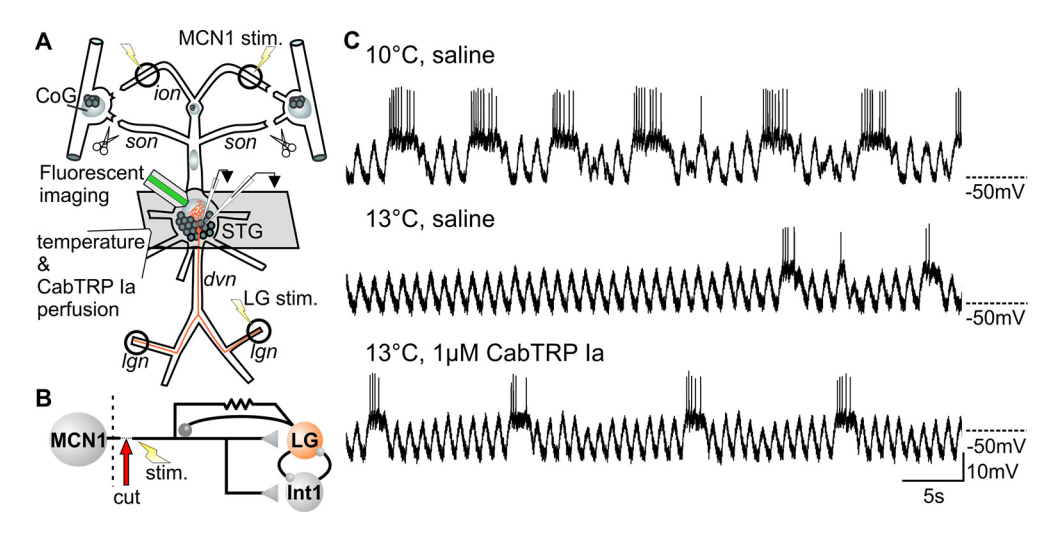


Figure 1. Rhythmic bursting of LG is interrupted by an acute temperature increase but can be restored by neuropeptide modulation. *A,* Schematic of the stomatogastric nervous system. Nerve names are italicized. In all experiments, *ions* and *sons* were transected. To elicit electrical postsynaptic potentials (ePSPs) in LG or initiate a gastric mill rhythm, the MCN1 axon was stimulated at either the left or right *ion*. For experiments where APs were measured, antidromic APs were initiated in the LG axon by stimulating one *lgn*. Electrical signals in LG were recorded intracellularly from the LG soma and extracellularly at the *lgn* not being stimulated. Antidromic AP and ePSP penetration into the LG neuropil was measured using calcium imaging. Temperature and CabTRP la modulation were applied focally inside a petroleum jelly well around the STG. *dvn*: Dorsal ventricular nerve. *B,* Circuit diagram underlying gastric mill rhythm generation. *C,* Example of intracellular LG recordings as MCN1 stimulation at 10 Hz generated rhythmic bursting in LG consistent with a gastric mill rhythm at 10°C (top), and failed to elicit bursts after an acute temperature increase of 3° C (middle). However, rhythmic bursting could be restored at 13°C with the addition of 1 μM CabTRP la applied to the well containing the STG (bottom).

associated with failures in respiratory neuronal activity resulting in sudden infant death syndrome in children and apneas in adults (Fleming et al., 1992; Tryba and Ramirez, 2004). In invertebrates, temperature changes have been shown to lead to failures of AP propagation and reduced synaptic effectiveness (Heitler and Edwards, 1998; DeMaegd and Stein, 2020). Possessing compensatory mechanisms that protect neurons from detrimental effects of temperature changes are thus vital components of survival.

Although circuit and cellular mechanisms for temperature compensation have been well described in a variety of systems (Tang et al., 2010; Robertson and Money, 2012; DeMaegd and Stein, 2020), they primarily address AP initiation and propagation in axons. Conversely, mechanisms for temperature compensation in neuropil regions are relatively unexplored, despite the importance of dendritic signal propagation and summation for AP initiation. Here, we identify a mechanism for temperature compensation of neuronal activity via neuromodulation of passive electrical spread in the dendrites of a motor neuron.

Recent studies indicate that neuromodulation can sustain neuronal activity at different temperatures (Städele et al., 2015; Zhu et al., 2018). Neuropeptides, in particular, have been implicated to support robust activity in pattern generating networks (Gray et al., 1999; Mutolo et al., 2010; Zhao et al., 2011; Shi et al., 2021). Our lab has shown that neuropeptide modulation supports rhythmic activity in the Cancer borealis gastric mill central pattern generator (CPG) as temperature increases (Städele et al., 2015). The gastric mill circuit controls mastication of food and is characterized by rhythmic AP bursts in the lateral gastric neuron (LG) as a necessary component of the rhythm. LG receives electrical and chemical synaptic input from the descending projection neuron modulatory commissural neuron (MCN1; Coleman et al., 1995; Stein et al., 2007). In in vitro assays, tonic MCN1 activity elicits strong LG bursts, but as temperature rises by only a few degrees, leak conductance increases, and bursts become shorter and less frequent and eventually fail. Activity can be sustained through the actions of the substance-P-related neuropeptide Cancer borealis tachykinin related peptide Ia (CabTRP Ia)

when bath applied or neuronally released. These actions are suspected to bestow a much greater temperature robustness to the gastric mill rhythm *in vivo* (Städele et al., 2015). However, the cellular mechanism by which this peptide acts to restore activity has of yet remained elusive.

We hypothesized that the loss of LG neuronal activity at a warmer temperature is because of reduced dendritic electrical spread in the LG neuron. Additionally, we hypothesized that CabTRP Ia restores rhythmic bursting by counterbalancing membrane shunt and increasing dendritic electrical spread. Using optical imaging and electrophysiology, we show that passive propagation of synaptic potentials and backpropagating APs is diminished in the LG neuropil with an acute temperature shift from 10 to 13°C but is restored when modulated by CabTRP Ia. Furthermore, we build on previous results indicating that membrane shunt increases from 10 to 13°C (Städele et al., 2015) to show that CabTRP Ia counterbalances membrane shunt at either temperature. Finally, we show that the modulator-induced (I_{MI}) current, the ionic conductance CabTRP Ia activates, is sufficient to restore passive propagation and rhythmic bursting by using a dynamic clamp protocol and applying an alternative peptide that activates I_{MI}. These data suggest that the mechanism of temperature compensation we describe is generalizable. Altogether, our data demonstrate that neuropeptide modulation of passive dendritic propagation sustains neuronal activity during acute temperature perturbations.

Materials and Methods

Dissection and solutions

Adult male crabs (Cancer borealis) were purchased from the Fresh Lobster Company and maintained in artificial sea water (salt content $\sim\!1.024\times {\rm g/cm^3},$ Instant Ocean Sea Salt Mix) at $10\text{--}11^{\circ}{\rm C}$ with a 12 h light/dark cycle. Animals were anesthetized on ice for 40 min before dissection. The stomatogastric nervous system was removed from the animal following standard procedures (Gutierrez and Grashow, 2009) and pinned out in a silicone-lined Petri dish (Sylgard 184, Dow Corning) for physiological studies (Fig. 1A). The nervous system was continuously

superfused (7-12 ml/min) with physiological saline containing the following (in mM): 440 NaCl, 26 MgCl₂, 13 CaCl₂, 11 KCl, 11.2 Trisma base, 5 Maleic acid, pH 7.4-7.6 (Sigma-Aldrich). In all experiments, the left and right inferior esophageal nerve (ions) and superior esophageal nerves (sons) were transected near the commissural ganglia (CoGs; Fig. 1A). A petroleum jelly well was built around the stomatogastric ganglion (STG) to allow for focal superfusion of modulators and temperature changes. One μ M CabTRP Ia (GenScript) and 0.1 to 0.5 μ M Crustacean Cardioactive Peptide (CCAP; Bachem; Swensen and Marder, 2000; DeLong et al., 2009b) were prepared from concentrated stock solutions immediately before bath application to the STG. Measurements were taken after 30 min of wash in. Temperature was altered between 10 and 13°C by chilling or warming superfused saline using Peltier devices (rate 1°C/min). Temperature was continuously monitored with a temperature probe (Voltcraft 300K, Conrad Electronic). Measurements were taken immediately after the temperature stabilized (typically <1 min after reaching the desired temperature).

Extracellular stimulation

Extracellular stimulation was performed using standard procedures (Städele et al., 2017). Small sections of nerves were electrically isolated from the surrounding bath using petroleum jelly wells. To elicit electrical postsynaptic potentials (ePSPs) in the LG neuron, the left or right ion was stimulated at 1-2 Hz (1 ms pulse duration; Master-8 stimulator, AMPI). The ion contains only two axons that project to the STG, those of the MCN1 and MCN5, respectively. The MCN1 axon has a lower stimulation threshold and thus can be selectively stimulated (Coleman et al., 1995). Stimulating the MCN1 axon with <2 Hz results in a negligible release of the MCN1 peptide cotransmitter CabTRP Ia as no slow sustained changes to the LG membrane potential are observed (Stein et al., 2007). None of the other MCN1 cotransmitters affect the LG neuron. However, each MCN1 axon stimulation results in a unitary ePSP of a several millivolt amplitude that is independent of MCN1 transmitter release (Coleman et al., 1995). We confirmed MCN1 was selectively stimulated by increasing stimulation voltage until an ePSP in LG was obtained. Additionally, we monitored the activity of the lateral pyloric neuron, which is inhibited by MCN5 (Norris et al., 1996). Preparations where MCN1 could not be selectively activated were not used for experimentation.

In experiments where a gastric mill rhythm was elicited, the stimulation frequency of an individual MCN1 was increased in 1 Hz steps until a gastric mill rhythm was observed at 10°C. This method of eliciting a gastric mill rhythm is standard protocol (Städele et al., 2015), and this version of the rhythm is easily identifiable (Coleman et al., 1995; Stein et al., 2007; Hedrich et al., 2011). The necessary frequency to elicit a gastric mill rhythm determined at 10°C was maintained at 13°C and during modulation to determine whether a gastric mill rhythm could be elicited.

In experiments where back propagating APs invaded the LG neuropil, we stimulated the LG axon distantly from the STG on the lateral gastric nerve (lgn; Fig. 1A). As before, a petroleum jelly well electrically isolated a small section of the lgn from the rest of bath, and the LG axon was stimulated at 1–2 Hz (1 ms pulse duration).

Electrophysiological recordings

Extracellular recordings were performed using standard procedures (DeMaegd et al., 2017). Extracellular signals were recorded, amplified, and filtered using an A-M Systems amplifier (Model 1700) and digitized with a Power1401 (Cambridge Electronics Design).

Intracellular recordings were taken directly from the LG soma using 20–30 $\rm M\Omega$ glass electrodes (Sutter 1000 puller, 0.6 M $\rm K_2SO_4+20$ mM KCl solution). For dye injections, electrodes were backfilled with Calcium Orange Tetrapotassium Salt (Invitrogen). To reduce background fluorescence noise from the activation of other neuronal processes in the neuropil, the dye was iontophoretically injected into the LG soma rather than bath applied. Injections were conducted using repetitive negative current pulses ranging from -3 to -5 nA (1–2 s pulse duration) for 30 min. The dye was allowed to diffuse throughout the neuronal processes before imaging. The LG soma was identified by the

occurrence of ePSPs timed to MCN1 stimulation and APs timed with spikes on the LG axon recorded from the lgn.

In some experiments, the LG resting membrane potential was held constant in a current clamp. Here, variable holding currents were applied through one of the two electrodes to maintain membrane potentials between -45 and -50 mV. In a few experiments, ePSP and AP amplitude were measured when the resting membrane potential was additionally held at -65 mV to determine whether the holding potential value affected our results. Although the amplitude values were smaller (consistent with Coleman et al., 1995), the qualitative change in amplitude in response to temperature and peptide modulation was similar. The same holding membrane potential used in current-clamp measurements of ePSP and AP amplitude was used in two-electrode voltage-clamp measurements of ePSC and AP current amplitudes. Signals were recorded, amplified, and filtered using an Axoclamp 900A amplifier (Molecular Devices).

Optical imaging

Fluorescent imaging of the LG neuropil was taken with the MiCAM02 imaging system using BVAna Software (version 13.07.04.8, SciMedia), using a 20× objective (XLUMPLFLN20XW, WD 2 mm, numerical aperture 1, Olympus) mounted on an upright epifluorescence microscope (modified BX51, Scientifica). Image resolution was 384 imes 256 or 192 imes128 pixels, sampled at a frame rate of 50 Hz. The region imaged was selected to encompass the majority of the LG neuropil in a single plane based on high-resolution images of the LG neuropil (Fig. 2A,F). To improve signal-to-noise ratio, optical signals were time-aligned to either MCN1 (for ePSPs) or LG axon (for APs) stimulation and averaged (Städele et al., 2012). For each condition and temperature, 20 trains of 2 Hz stimuli (3 s duration per train) were elicited. The first and last stimulus of each train was discarded to avoid potential onset and end-of-recording artifacts of the camera. This resulted in a total of 100-150 stimuli, which were averaged for each condition. Individual signals were first averaged across trains and then further averaged within each train. In addition, the resulting fluorescence images were processed with the BVAna software spatial average function that averages the fluorescence of 3×3 pixels (SciMedia). Excitation illumination was provided by the pE-400 luminance system (CoolLED) at 550 nm and filtered with 605 nm/670 nm bandwidth excitation filters. Light levels were adjusted to optimize signal-to-noise ratio and avoid phototoxicity or photobleaching.

Two measurements of electrical spread were quantified using the optical imaging data, fluorescence area and fluorescence intensity. The total fluorescent area was determined by converting the pseudocolor images to black-white images based on a 70% intensity threshold. Other thresholds (50-90%) were tested but revealed no qualitative differences. Gray regions of Figure 2, B and G, represent pixels that did not exceed the threshold, whereas all other colors exceeded the threshold. Pixels exceeding the intensity threshold were counted using an original script (Mathematica, Wolfram) or using the count function of the FIJI processing package (Schindelin et al., 2012). For all measurements, the baseline fluorescence at time = 0 ms (frame 0) was subtracted to account for changes in background fluorescence. As pixel numbers differed largely among individual preparations because of the varying background fluorescence and dye distribution in the neuropil, data for each preparation were normalized to the average change of all experimental conditions in that experiment. The fluorescence intensity was measured as the mean fluorescence within the selected region of interest (the neuropil area of LG, see above). The largest deviation from baseline fluorescence was then used to compare among experimental conditions. Because fluorescence intensity differed largely among individual preparations because of varying dye distribution in the neuropil, data for each preparation were normalized to the average change in fluorescence of all experimental conditions in that experiment.

Dynamic clamp

Dynamic clamp experiments were used to inject an artificial $I_{\rm MI}$ conductance into LG in two-electrode current-clamp mode (Sharp et al., 1993) using Spike 2 software (CED) to calculate current slope. All other

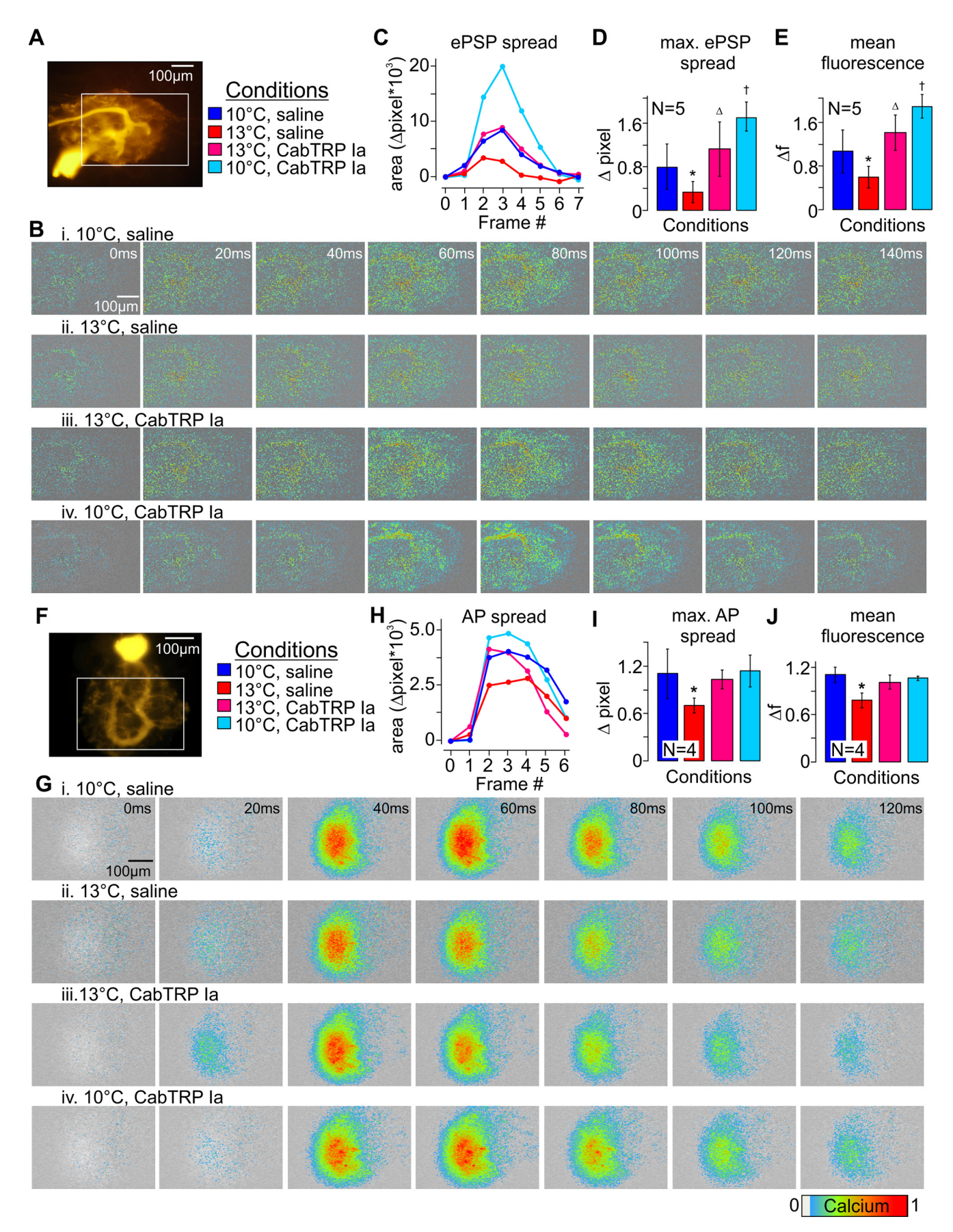


Figure 2. Temperature and neuropeptide modulation alter ePSP and AP-induced calcium spread in the LG neuropil. **A**, The LG soma was iontophoretically injected with a fluorescent calcium indicator, which was allowed to diffuse throughout the neuropillar processes. The white box indicates the region of interest selected for imaging and analyses. **B**, Time series of pseudocolored images of calcium fluorescence concurrent with ePSPs in the LG neuropil. Warmer colors represent higher intensity fluorescence and greater calcium concentrations. Background luminance

calculations were performed in the Spike2 Sequencer using a Power1401 AD converter (CED). An $I_{\rm MI}$ model was developed based on previously published descriptions of $I_{\rm MI}$ (DeLong et al., 2009b; Städele et al., 2015) using the following equation:

$$I = \overline{g} * a^P * (V - E),$$

with g being the maximum conductance (nS), a being the activation (ms), p=1, E being the equilibrium potential (mV), and V being the membrane potential (mV). In our implementation, the activation was instantaneous and \bar{g} was varied between 0, 25, 50 nS. To reduce computational load in the Spike2 Sequencer, the voltage–current relationship was implemented using piecewise linear approximation as follows:

at
$$V < -70$$
, $I_{MI} = 0$
at $-70 \le V \le -40$, $I_{MI} = -0.7 * \bar{g} * (V + 70)$
at $-40 \le V \le -20$, $I_{MI} = -0.7 * \bar{g} * (-40 + 70)$
at $V > -20$, $I_{MI} = \bar{g} * (V - 0)$.

Input resistance

Input resistance was calculated by measuring the change in current when LG was hyperpolarized by $10\,\mathrm{mV}$ from $-50\,\mathrm{mV}$ using a two-electrode voltage clamp. Input resistance was calculated using the following equation:

$$R = V/I$$
,

where R is input resistance $(M\Omega)$, I is the change in current (nA), and V is the change in membrane potential (mV).

Model

The influences of changes to leak conductance and synaptic strength on (1) ePSP amplitude and (2) AP amplitude were modeled with NEURON (Hines and Carnevale, 2001; available from ModelDB (accession 266881) at http://modeldb.yale.edu/26688). In both types of experiments, we measured amplitudes after signals passively propagated 500 μm and 1250 μm along an unbranched neurite (2.5 μm diameter, 4000 μm total length, $1\,\mu m$ compartments, $R_a=100~\Omega cm,~C_m=1~\mu F/cm^2).$ These values approximated the properties of STG motor

(gray) was determined by a threshold set to 70% of the peak fluorescence. \boldsymbol{c} , Quantification of fluorescent area (pixels) for each time point of each condition shown in **B**. **D**, Quantification of ePSP penetration in the LG neuropil represented by the change in fluorescent area (N = 5, data includes the example LG in A-C). Data were normalized to the average of all conditions, in each preparation. E, Quantification of ePSP penetration represented by the change in mean fluorescence intensity for each condition (N = 5). Data were normalized to the average of all conditions in each preparation. F, In a separate experiment, the LG soma was iontophoretically injected with a fluorescent calcium indicator, and APs were elicited by stimulation of the Ign. APs propagated antidromically toward the neuropil and soma, and passively spread in the neuropil. G, Time series of pseudocolored images of calcium fluorescence concurrent with APs in the LG neuropil in the same location as depicted by the white box in F. H, Quantification of fluorescent area (pixels) for each time point of each condition shown in G. I, Quantification of AP penetration in the LG neuropil represented by the change in fluorescent area (N=4, data includes the example LG in F-H). Data were normalized to the average of all conditions in each preparation. J, Quantification of AP penetration represented by the change in mean fluorescence intensity for each condition (N = 4). Data were normalized to the average of all conditions in each preparation. *significant difference (p < 0.05) from all other conditions. Δ significant difference (p < 0.05) from 13°C saline and 10°C CabTRP Ia. †significant difference (p < 0.05) from 10°C saline.

neurons (Nadim et al., 1998). The neurite did not contain any active properties, making all signal propagation passive.

In experiments where ePSP amplitude was measured, the neurite contained a linear passive leak current with a constant equilibrium potential (-60 mV) but variable maximum conductance values (73.0, 76.7, 80.3, 84.0, 94.9, 110.0 µS/cm²). These values represent a conductance increase of 0, 5, 10, 15, 30, and 50%, which covers the approximate range of changes in membrane resistance measured in the LG neuron from 10° to 13° C. To simulate a postsynaptic potential from an ePSP, we injected brief current pulses (1 ms) at 5 µm from the origin of the neurite. To model a temperature-dependent change in synaptic strength, the amplitude of the current injection was varied in several steps (0.20, 0.21, 0.22, 0.23, 0.26, 0.30) representing an increase of 0, 0.5

In experiments where AP amplitude was measured, a 1000-µm-long axon with active properties was attached to the neurite to initiate APs. Active conductances were modeled with Hodgkin-Huxley equations (Hodgkin and Huxley, 1952b) and included a voltage-gated sodium channel (equilibrium potential 45 mV and maximum conductance 40 mS/cm²), voltage-gated potassium channel (equilibrium potential -80 mV and maximum conductance 6.0 mS/cm²), and a passive leak channel (equilibrium potential -60 mV and maximum conductance 73.0 μS/cm²). APs were elicited 500 μm away from the origin of the neurite by injection of 1.5 nA current pulses (1 ms pulse duration). APs propagated actively along the axon toward the neurite and continued passively within the neurite. As in the aforementioned experiments, the maximum leak conductance was varied in the neurite between 73.0 and 110.0 μS/cm². To assess the influence of temperature-dependent changes in AP sodium current on AP voltage amplitude, we varied the maximum conductance of the voltage-gated sodium channel among 40, 42, 44, 46, 52, 60 mS/cm², corresponding to an increase of 0, 5, 10, 15, 30, and 50%. Although this did not include temperature-dependent influences on activation and inactivation (Hille, 2001), increasing the maximum conductance over this broad range includes potential changes to the sodium current that occur as a result of changes in gating time constants. Nevertheless, we additionally measured the effect of temperature on AP amplitudes using the NEURON temperature distributed mechanism, which modifies the activation rates of all active conductances. These experiments revealed qualitatively similar results to varying the maximum sodium conductance alone (data not shown).

Experimental design, data analysis, and statistical analysis

Electrophysiological files were recorded, saved, and analyzed using Spike2 (version 7.18, CED) and original scripts (http://www.neurobiologie.de/spike2).

We used parametric (ANOVA) and nonparametric tests (ANOVA on ranks). In cases where different variables were measured in individual animals, repeat measures were considered (for factors and specific designs of each ANOVA, see below, Results). Statistical tests were performed using SigmaStat (version 11, Systat Software). Statistical tests are reported in the following format: statistical test, $F_{\text{(degrees of freedom, residual)}} = F$ value, p value, p ost hoc test, number of experiments. An uppercase N denotes the number of preparations, and a lowercase n denotes the number of trials. Exact p values are provided unless they were smaller than 0.001. P ost hoc tests are at a significance level of 0.05 unless otherwise noted. Data were prepared in Excel and finalized in CorelDRAW (version X7). In figures, data are presented as mean \pm SD. Individual animal responses are plotted beside the average and connected by a line when recorded in multiple conditions to indicate paired data.

Results

Before measuring the spread of electrical signals in LG, we ensured that the previously published effects of temperature on LG were present in each tested animal. We decentralized the STG to remove spontaneous extrinsic modulation from descending projection neurons in the CoGs by cutting the *sons* and *ions*. The STG, where the LG soma is located, was isolated with a

petroleum jelly well and superfused with different-temperature saline, either with or without CabTRP Ia (Fig. 1A, see above, Materials and Methods). The rest of the stomatogastric nervous system was held at a constant temperature. We recorded LG activity intracellularly. To elicit the gastric mill rhythm, we extracellularly stimulated an individual MCN1 axon at 10°C. Tonic stimulation of MCN1 activates a gastric mill rhythm through chemical excitation of LG and Interneuron 1, and an electrical synapse with LG (Fig. 1B). Figure 1C shows rhythmic LG activity after 50 s of tonic MCN1 stimulation (top, 10°C). In saline, LG activity diminished with increasing temperature, and the gastric mill rhythm failed at 13°C (middle). However, in the presence of 1 μ M CabTRP Ia (bottom) rhythmicity was restored at 13°C. These results matched those previously reported (Städele et al., 2015).

Passive propagation in the LG neuropil depends on temperature and neuromodulation

We used a fluorescent calcium indicator to determine whether passive propagation in LG dendrites decreases at warmer temperatures. We iontophoretically injected the indicator (calcium orange) into the LG soma and allowed it to diffuse throughout the LG neuropil. An example of a stained LG neuron is shown in Figure 2A. Then, we elicited individual ePSPs through extracellular stimulation of the MCN1 axon (see above, Materials and Methods; Coleman et al., 1995). To avoid potential confounding influences of the MCN1 neurotransmitters, we used a low stimulus frequency (1–2 Hz). At this stimulation frequency, LG shows no response to MCN1 neurotransmitters (Stein et al., 2007) but displays a several millivolt large ePSP with each MCN1 stimulation (Coleman et al., 1995). These ePSPs do not contribute to the initiation of the gastric mill rhythm (Coleman et al., 1995; Bartos et al., 1999) and because of their electrical nature, they are independent of the presence of presynaptic or postsynaptic calcium. They thus offer a convenient way to quantify the area of the neuropil that electrical signals disperse across, or in other words, the spread of electrical signals through the LG neuropil. We used this fact to test how well synaptic potentials penetrate the neuropil at different temperatures and in the presence of neuropeptide modulation. Figures 2B, shows a time series of pseudo-colored images of Calcium fluorescence in a single plane of the LG neuropil after MCN1 stimulation, imaged at 10°C. Each image represents the average fluorescence of 100-150 stimuli at the indicated time point. The highest intensity fluorescence was located approximately in the center and diminished in the surround, indicating that this region either had the greatest accumulation of calcium or the greatest number of gap junctions. There was a clear increase in both fluorescence intensity and neuropil area covered by the fluorescence signal, illustrating the extent of ePSP propagation within the neuropil. Specifically, the ePSP first occurred at 20 ms. Its spatial spread increased until 60 ms and then slowly diminished back to baseline levels. Figure 2C (dark blue line) shows the spatial extent of the calcium signal throughout the neuropil by measuring the pixel number covered by the fluorescence signal. We arbitrarily set a threshold of 70% of the maximum fluorescence in each set of experiments to assign either a value of 0 (below threshold) or a value of 1 (equal or above threshold) to each pixel (see above, Materials and Methods). Changes in pixel number from the time of stimulation (time = 0, frame = 0) were then plotted over time and taken as an indicator for the total fluorescent area (Fig. 2C). In all conditions tested, we found that the fluorescent area increased shortly after MCN1 stimulation, reached a peak, and then shrunk again, clearly demonstrating that ePSPs extended throughout the LG neuropil in a time-dependent manner. We predicted that as temperature increases, the fluorescent area would decrease, consistent with diminished electrical spread in the neuropil. Indeed, at 13°C, the fluorescent area was smaller than at 10°C (Fig. 2B, ii, 2C, red line).

To assess whether neuropeptide modulation increases electrical spread, we bath applied 1 μ M CabTRP Ia and compared the fluorescent area to the saline condition. The LG neuropil showed a larger region of fluorescence and an increase in warmer colors when CabTRP Ia was added at 13°C (Fig. 2B, iii, C, pink line) than at 13°C in saline (Fig. 2B, ii, C, red line), indicating a wider spread of the ePSP with CabTRP Ia modulation. We found a similar result for 10°C, when we compared the 10°C CabTRP Ia condition (Fig. 2B, iv, C, light blue line) with its saline control (Fig. 2B, i, C, dark blue line).

To compare ePSP propagation distance in the different conditions across animals, we compared the maximum area (the largest value in Fig. 2C) in each condition, for each animal (Fig. 2D). There was a significant change in fluorescence area across conditions (ANOVA on ranks, $H_{(3\)}=12.406,\ p=0.006$). Student–Newman–Keuls method pairwise comparisons (p<0.05) revealed significant differences among all conditions with the exception of 13°C CabTRP Ia and 10°C saline.

To further confirm our results, we additionally analyzed the intensity of the fluorescence signal across conditions and animals. Here, instead of counting pixels, we measured the mean fluorescence intensity in all of the LG neuropil in the image frame with the highest fluorescence intensity. Specifically, we selected the LG neuropil as the region of interest (Fig. 2A, white box) and measured mean fluorescence within this region for each image frame of the time series. The maximum value of this analysis was then recorded and compared across animals. Figure 2E shows the results of this analysis, which revealed the same significances as in Figure 2D. There was a significant difference between conditions (ANOVA on ranks, $H_{(3)} = 13.674$, p =0.003). Specifically, Student-Newman-Keuls method pairwise comparisons (p < 0.05) revealed that all conditions were significantly different from one another, except for 13°C CabTRP Ia and 10°C saline. Together, these data suggest that the propagation of the ePSPs was reduced at the warmer temperature but also that neuropeptide modulation increased electrical spread in both temperature conditions.

Although these data support the hypothesis that electrical spread diminished at warmer temperatures and was restored by peptide modulation, they do not conclusively demonstrate that a shunt in the LG neurites contributed to the reduction of the electrical spread. Temperature-mediated effects on LG synaptic input, either directly through changes to synaptic current or indirectly through the hyperpolarization of the LG resting membrane potential (Coleman et al., 1995), may additionally alter ePSP penetration into the LG neuropil. As a first step to address this issue, we considered an additional way to test the spread of electrical signals in the LG neuropil. Here, we measured the passive propagation of APs throughout the neuropil, which had invaded antidromically from the axon. Measuring passively propagating APs has the advantage that they do not depend on potentially temperature-sensitive synaptic currents nor are they affected by potentially confounding actions of synaptic calcium currents. Because the membrane potential must cross a threshold potential when eliciting an AP and because APs have a large amplitude when elicited in the axon (Ballo et al., 2012), a few millivolt hyperpolarization of the resting membrane potential will

have little influence on total AP amplitude. Additionally, when elicited in the axon, AP amplitudes are mostly determined by the sodium equilibrium potential and less by the sodium current (Hodgkin and Huxley, 1952a). AP amplitudes should thus be less sensitive to temperature-induced changes in AP currents.

In these experiments, APs were initiated via extracellular stimulation of the *lgn* at low frequencies (1–2 Hz, Fig. 1A; see above, Materials and Methods). Figure 2, F and G, shows an example experiment, where the LG neuropil was again stained with a calcium dye. Figure 2G shows the associated time series of pseudocolored images of calcium fluorescence for the different conditions this neuron was exposed to. Figure 2, H–J, shows the same analyses as performed for the ePSPs in Figure 2, C–E. APs invaded the main LG neurite, and although the calcium signal was strong, its spread was less than that for the ePSPs. This is consistent with earlier findings that antidromic APs have limited access to the neuropilar segments of STG neurons (Mulloney and Selverston, 1972; Meyrand et al., 1992). However, similar to our observations for the ePSPs, the penetration into the neuropil was reduced at 13°C when compared with 10°C (Fig. 2G, i, ii), indicated by smaller fluorescent regions). Figure 2H shows the quantification of the fluorescent area (dark blue, 10°C; red, 13°C).

When modulated by CabTRP Ia, at 13°C, the neuropil area penetrated by the APs increased in comparison to the saline condition and remained increased when the temperature was reduced to 10°C (Fig. 2G, iii, iv, 2H, pink and light blue traces). These results were consistent across animals, and there was a significant change in fluorescent area across conditions (ANOVA on ranks, $H_{(3)} = 8.096$, p = 0.044). Student-Newman-Keuls method pairwise comparisons (p < 0.05) revealed that the 13°C saline condition was significantly different from all other conditions (Fig. 21). Measuring fluorescence intensity (Fig. 21) across animals resulted in the same result, with significant changes in fluorescence across conditions (ANOVA on ranks, $H_{(3)} = 8.603$, p = 0.035), with the 13°C saline condition being significantly different from all other conditions (Student-Newman-Keuls method pairwise comparisons, p < 0.05). Like in the experiments with ePSPs, the 10°C CabTRP Ia condition tended to show the largest fluorescent area and intensity, however this difference was not significant. This could be the result of the generally smaller area the AP penetrates and the higher fluorescence intensities it causes, making detecting small differences more difficult. Nevertheless, together, both the AP and ePSP results support the hypothesis that electrical spread in the LG neurites decreases at warmer temperatures and that CabTRP Ia modulation restores or even enhances this spread. These effects of temperature can at least in part be attributed to a shunt of the LG membrane.

To further ascertain that membrane shunt reduces the spread of electrical signals in LG, we electrophysiologically recorded ePSPs and antidromic APs as they arrived in the soma, after passively propagating through parts of the neuropil. We used a two-electrode current clamp to determine ePSP and AP amplitudes.

The electrical synapse between MCN1 and LG had previously been shown to be voltage dependent, such that more hyperpolarized membrane potentials reduce the ePSP amplitude (Coleman et al., 1995). To avoid additional voltage-dependent influences on our measurements, we maintained a constant resting membrane potential at all temperatures (see above, Materials and Methods). We used the same stimulation protocol as for our optical imaging experiments. Like for other STG motor neurons, APs stimulated in the LG axon passively and antidromically

propagate toward the soma, with considerable loss in amplitude when they arrive (Mulloney and Selverston, 1972; Meyrand et al., 1992). We found that AP amplitude diminished from 10 to 13°C (Fig. 3A, top, blue and red traces, respectively). This was a consistent observation across all animals [Fig. 3A, bottom, one-way repeated-measures (rm)ANOVA, $F_{(6,3)} = 32.378$, p < 0.001; Student–Newman–Keuls method; 1 C vs 13°C, p < 0.05, N = 7]. In CabTRP Ia, AP amplitude at 13°C recovered and was no longer different from the 10°C saline condition (Fig. 3A, top, pink trace; bottom, Student-Newman-Keuls method, 13°C CabTRP Ia vs 13°C saline, p < 0.05; 13°C CabTRP Ia vs 10°C saline, n.s.). When we lowered the temperature back to 10°C in CabTRP Ia, AP amplitude increased further and was then larger than in the respective saline control (Fig. 3A, top, light blue trace; bottom, Student-Newman-Keuls method; 10°C CabTRP Ia vs 10°C saline, p < 0.05). These results are consistent with the prediction that increased temperature diminishes passive spread of electrical signals in LG and that CabTRP Ia modulation increases the spread.

For ePSPs, we found that there was a significant change in amplitude across conditions (one-way rmANOVA, $F_{(6,3)}$ = 11.520, p < 0.001). However, ePSP amplitude was not significantly altered when the temperature was increased from 10 to 13°C in saline (Fig. 3C, bottom, Holm–Sidak multiple comparisons, 10°C saline vs 13°C saline, n.s.), although in a few cases ePSP amplitude increased (Fig. 3C, top, compare blue and red traces). In CabTRP Ia, ePSP amplitudes increased further, such that at each temperature they were significantly larger than the respective saline controls (Fig. 3C, top, pink and light blue traces; bottom, Holm–Sidak multiple comparisons, 13°C saline vs 13°C CabTRP Ia, p < 0.05; 10°C saline vs 10°C CabTRP Ia, p < 0.05).

The above results were contrary to our prediction that ePSP amplitude would decrease from 10° to 13°C in saline because of a shunt along the neurite. They also do not align with our optical imaging data that indicate reduced ePSP propagation in the neuropil. This suggested that additional factors influence ePSP amplitude. Specifically, synaptic input could be affected by temperature and/or CabTRP Ia modulation. To address these issues, we used a two-electrode voltage clamp to measure the ePSC of the MCN1-LG synapse. The membrane potential was held at the same potential used for the measurements of ePSP and AP amplitudes, while the MCN1 axon was stimulated at low frequency (1 Hz). The current needed to maintain the holding potential changed from 10° to 13°C in saline and 1 μ M CabTRP Ia, consistent with a change in membrane shunt. However, because we were interested in changes in synaptic current, Figure 3D (top) shows the average traces of 20 ePSCs in each of the four different conditions aligned to the same baseline current. We found that ePSC amplitude significantly increased from 10° to 13°C in saline (Fig. 3D, top, blue and red traces; bottom, one-way rmANOVA, $F_{(6,3)} = 5.273$, p = 0.009; Student-Newman-Keuls method pairwise comparisons, 10°C saline vs 13°C saline, p < 0.05), indicating that the synaptic current increases with temperature. This temperature-induced increase in synaptic current antagonizes the influence of membrane shunt on ePSP amplitude.

CabTRP Ia modulation had no further influence on ePSC amplitude at either temperature (Fig. 3D, top, compare dark and light traces; bottom, Student–Newman–Keuls method, 13°C saline vs 13° CabTRP Ia, n.s.; 10°C saline vs 10°C CabTRP Ia, n.s.), suggesting that CabTRP Ia does not increase ePSP amplitude by altering synaptic current.

For antidromic APs, we found that although again the current necessary to maintain the holding potential changed with temperature and peptide modulation, the AP current amplitude was not significantly affected by a temperature increase from 10° to 13°C (Fig. 3B, top, blue and red traces) or by CabTRP Ia modulation (Fig. 3B, top, compare light and dark traces; bottom, one-way rmANOVA, $F_{(6,3)} = 0.569$, n.s.).

Our optical and electrophysiology data thus indicate that APs penetrate the neuropil less because of the temperature-induced shunt. The situation for the ePSPs is less clear because membrane shunt and synaptic current appear to compete. To assess how this competition affects the ePSP amplitude, we built a computational model neurite, which allowed us to measure ePSP amplitude given different levels of synaptic current and membrane shunt. The model consisted of a 4000-µm-long unbranched neurite that possessed only passive properties (maximum leak conductance (g_{Leak}), 73.0 μS/cm²; see above, Materials and Methods). To simulate the synaptic current of an electrical synapse like the one between MCN1 and LG, we injected a 1 ms 0.2 nA current pulse at 5 µm from the neurite origin. The elicited voltage change had a similar amplitude and time course as an ePSP in the LG neuron. To measure passive ePSP propagation along the neurite, ePSP amplitude was recorded at 500 µm and 1250 µm away from the ePSP initiation site. Figure 4A, i and ii, shows the ePSPs with the baseline conditions (blue traces). As expected for passive propagation, ePSP amplitude diminished with longer distances from ePSP origin.

To test the individual effects of temperature-induced increases in leak conductance on passive propagation, we increased the leak conductance in steps from 73.0 to 110.0 µS/cm² over the entire length of the neurite (see above, Material and Methods). Similarly, to test the effects of temperature-induced increases to synaptic current, we increased current injection at the ePSP initiation site from 0.2 to 0.3 nA. Expectedly, ePSP amplitude was inversely proportional to the increase in maximum leak conductance but proportional to the synaptic current. Figure 4, A and B, shows that this was the case independently of whether ePSPs were recorded at 500 µm or 1250 µm. At either location, an increase in leak conductance diminished ePSP amplitude (compare blue and red traces, Fig. 4A, i, ii) and an increase in synaptic current increased the ePSP amplitude (com-

pare blue and pink traces, Fig. 4A, i, ii). Figure 4B, i and ii, quantifies the changes in amplitude relative to the baseline ePSP amplitude resulting from an increase in leak conductance (horizontal axis) or synaptic current (vertical axis) at both recoding locations. We found, however, that when the leak conductance and synaptic current were changed together, the resulting changes in ePSP amplitude were more challenging to predict. For example, when the leak conductance was increased by 30%, and the synaptic current was increased by 10% (purple traces, Fig. 4A, i, ii; purple circles, B, i, ii), ePSP amplitude at 500 µm

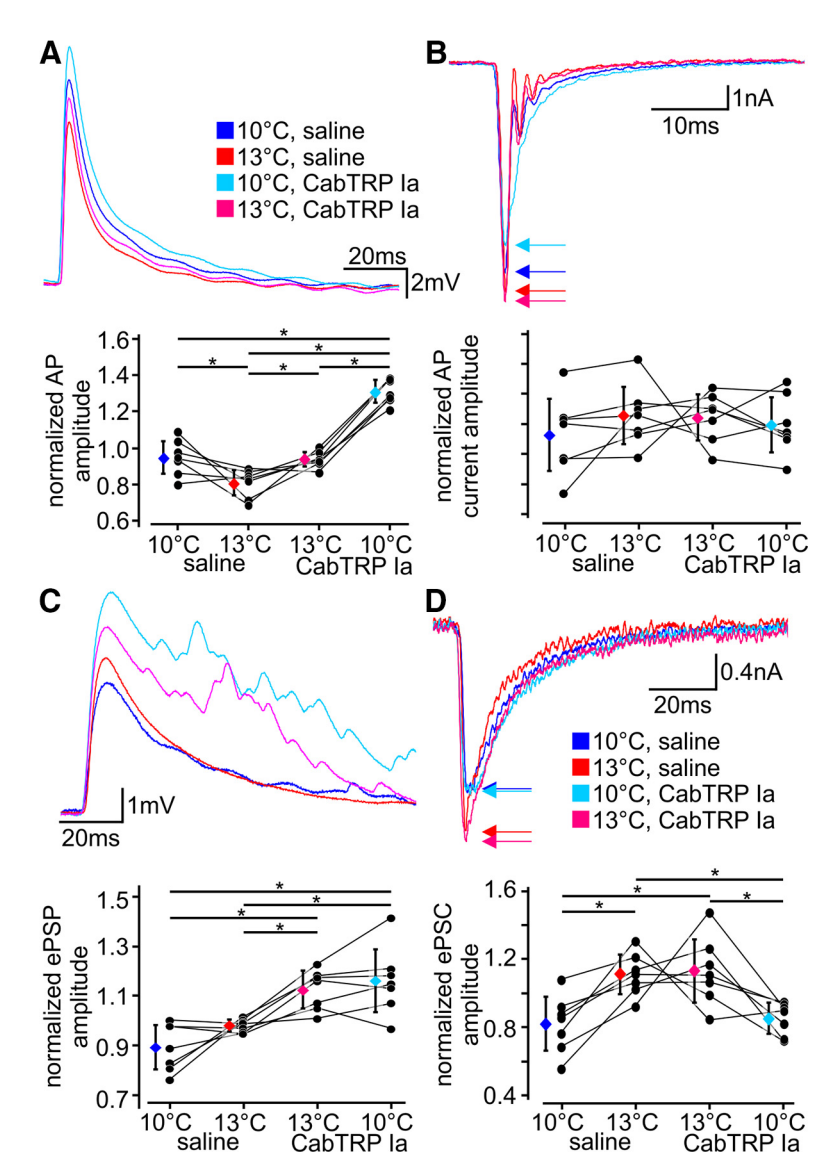


Figure 3. Temperature and neuropeptide modulation change ePSP and antidromic AP amplitudes. **A**, Top, Representative example of the average AP amplitude (n=20 APs/trace) measured from the LG soma at constant membrane potential. Amplitude was measured in saline at 10°C (blue) and 13°C (red), and in CabTRP la at 10°C (light blue) and 13°C (pink). Bottom, AP amplitude decreased significantly from 10°C to 13°C in saline and increased significantly in CabTRP la (N=7). Paired data from a single preparation are connected by lines. **B**, Top, Representative example of the average total AP current (n=20 APs/trace) in each condition. Bottom, There was no significant difference across animals in any condition. **C**, Top, Average ePSP amplitude (n=20 ePSPs/trace) measured from the LG soma at constant membrane potential in each condition. In the presence of CabTRP la, occasionally APs were elicited in response to ePSPs resulting in peaks in the ePSP tail. Bottom, Increasing the temperature from 10°C to 13°C did not significantly alter ePSP amplitude when the membrane potential was held constant. However, CabTRP la still increased ePSP amplitude. **D**, Top, Representative ePSC average amplitude for each condition (n=20 ePSCs/trace). Bottom, Across animals (N=7), ePSC amplitude increased with warming $(10^{\circ}\text{C}$ to $13^{\circ}\text{C})$ but was not affected by peptide modulation. *p<0.05.

increased from baseline, whereas at $1250~\mu m$ it decreased (compare blue and purple traces, Fig. 4A). Thus, the distance between the ePSP initiation site and recording site determined whether the ePSP amplitude increased or decreased relative to its baseline amplitude.

Specifically, at $500 \, \mu m$, very few combinations of parameters led to a decrease of ePSP amplitude (squares below the solid black line, Fig. 4B, i), and many combinations led to an increase (squares above the solid line). Whereas, at $1250 \, \mu m$, more combinations of parameters led to a decrease of ePSP amplitude. Figure 4B, ii, shows this by having more squares below the solid

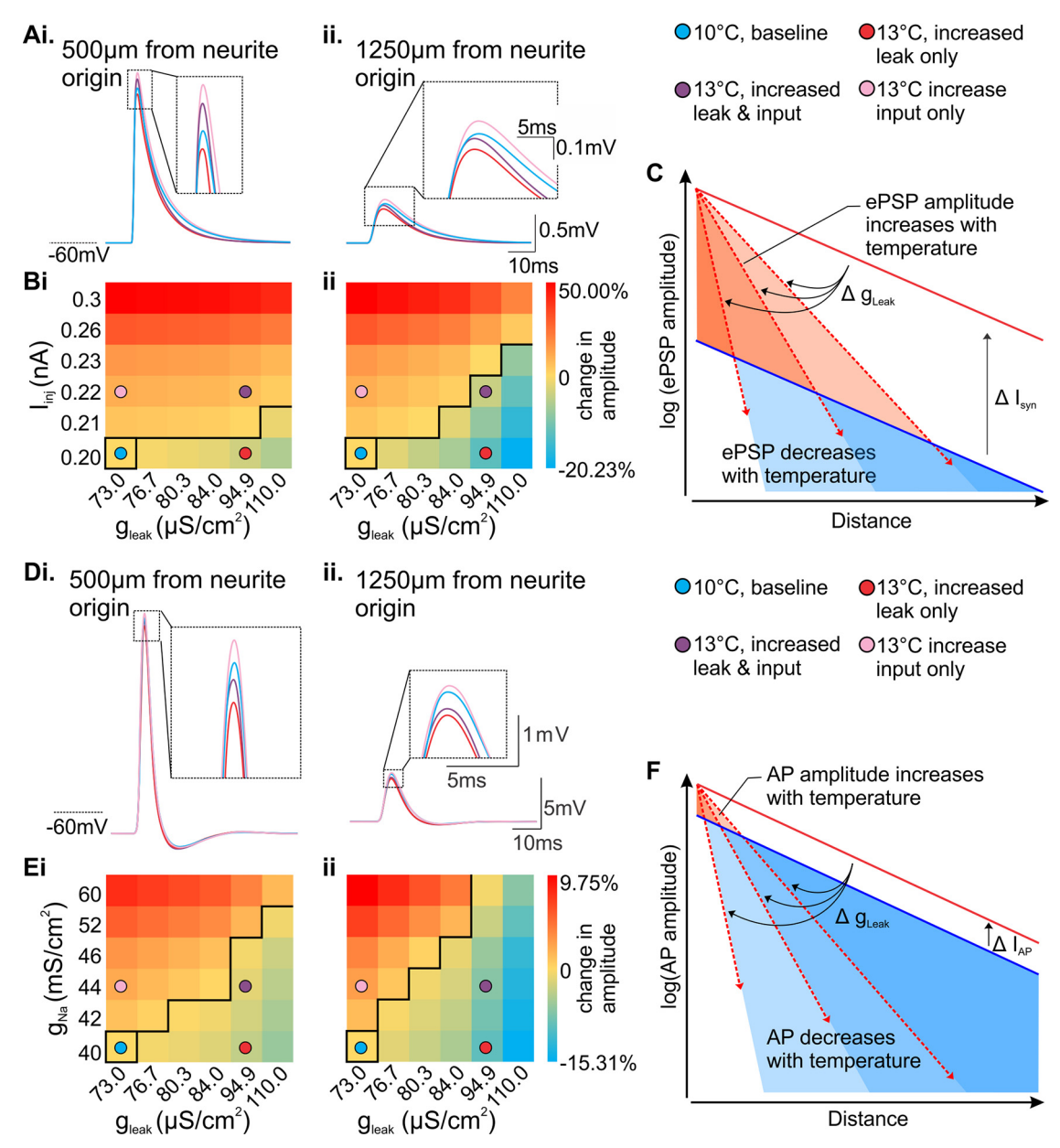


Figure 4. Membrane shunt and synaptic input have competing influences on signal amplitude. *A*, Example ePSP recordings at (i) 500 μm from the site of current injection and (ii) 1250 μm from the site of current injection. Blue traces represent the baseline ePSP (ePSP at 10°C; g_{Leak}: 73.0 μS/cm², l_{inj}: 0.2 nA). Red trace: ePSP at 13°C when only the leak conductance was increased (g_{Leak}: 94.9 μS/cm², l_{inj}: 0.2 nA). Purple trace: ePSP at 13°C when both influences occur simultaneously (g_{Leak}: 94.9 μS/cm², l_{inj}: 0.22 nA). At 500 μm, the ePSP was larger than the baseline ePSP, whereas at 1250 μm the ePSP was smaller, despite the same membrane shunt. Figure and inset scales are identical in *A* i and *A* ii. *B*, Percent change in ePSP amplitude relative to the baseline ePSP for different temperature-induced increases in leak conductance (horizontal axis) and injected currents (vertical axis). Measurements were recorded at 500 μm (i) and 1,250 μm (ii), like in Figure 4*A*. To allow for comparisons between recording sites, both heat maps are scaled to the same change in amplitude depicted in *B* ii. ePSPs larger than the baseline ePSP are recorded as positive values and are represented by warmer colors (red), whereas smaller ePSPs are recorded as negative values and are represented by cooler colors (blue). *C*, Schematic of the effects of synaptic current, leak conductance, and recording site distance on ePSP amplitude. *D*, Example recordings of APs that passively propagated through the neurite at the indicated locations (i, ii). Trace colors as described in *A* (blue, baseline AP at 10°C, g_{Leak}: 73 μS/cm², g_{Na}: 40 mS/cm²; pink, AP at 13°C dual increase only, g_{Leak}: 73 μS/cm², g_{Na}: 44 mS/cm²). For the same relative increase in both leak (30%) and input (15%) as shown for the ePSP in *A*, AP amplitude decreased at both recording locations (compare purple and blue trace amplitudes). Scales shown in *B* ii applies to *E* i as well. *F*, Schematic of the effects of a temperature-induced increase in to

line and generally cooler colors compared with Figure 4*B*, i. Importantly, this suggests that depending on where one records in the neurite, a temperature-induced increase in synaptic current can outweigh the diminishing effect of increased leak conductance on ePSP amplitude. This is particularly true at recording sites close to ePSP initiation sites. Figure 4*C* schematizes

this conclusion by showing how the ePSP amplitude depends on the weighting between increases in synaptic current and membrane shunt, as well as the recording location. Specifically, ePSPs measured distantly from initiation sites are more likely to decrease in amplitude at warmer temperatures, whereas when measured closer they are more likely to increase, even with the same change in membrane shunt. Somatic recordings in STG neurons have extraordinary electrical access to neuritic events and thus appear electrotonically close to synaptic inputs (Otopalik et al., 2017). This could explain the observed results that ePSP amplitude recorded from the soma did not decrease at 13°C. Instead of reflecting an increase in membrane shunt, ePSP amplitudes in the soma thus predominantly reflected the effect of increased synaptic current.

In contrast to the ePSPs, AP amplitude never increased in our electrophysiological experiments. This finding is consistent with an increase in membrane shunt but only a small increase in the maximum AP current within the 3°C temperature range tested in these experiments. However, the total current associated with the action potential can increase more with larger temperature changes (DeMaegd and Stein, 2020). To test possible interactions between such an increase and temperature-induced membrane shunt, we extended our previous computational model neurite and added a 1,000 µm axon with active properties (voltage-gated sodium and potassium channels, implemented via Hodgkin and Huxley (1952b) formalism; see above, Materials and Methods). In the axon section, APs could be elicited and propagated actively. APs were initiated with a short suprathreshold current injection (1 ms, 1.5 nA) in the middle of the axon, $500 \,\mu m$ from the origin of the passive neurite. After entering the neurite, the amplitude of the now passively propagating AP was assessed at the same two locations (500 µm and 1250 µm from the origin of the neurite). In baseline conditions, leak conductance in the neurite was set to 73.0 μ S/cm² (Fig. 4D, blue traces).

As expected for passive propagation, AP amplitude diminished with larger distances from the axon (Fig. 4D, i, ii, blue traces and more cooler colors in Fig. 4E, ii, than in i). We then sought to confirm the individual influences of a temperature-induced increase in membrane shunt and AP current on passive propagation. First, the leak conductance was increased from 73.0 to 110 $\mu \text{S/cm}^2$ in the neurite. Leak remained unaltered in the axon to not interfere with AP initiation. Figure 4D, i and ii (red traces), shows the example of a 30% increase in leak conductance (94.9 $\mu \text{S/cm}^2$). AP amplitude diminished in both locations. This was the case for all increases in leak conductance (Fig. 4E, i, ii, shift toward cooler colors along the horizontal axis).

To next determine how a temperature-dependent increase in AP current affects AP amplitude, we increased the sodium conductance (g_{Na}) from 40 to 60 mS/cm². This increased the total sodium current during the action potential and thereby the total AP current (data not shown). The pink traces in Figure 4D, i and ii, show the resulting AP after passively propagating to the two recording sites in the neurite, with a 10% increase in axonal sodium conductance ($g_{Na} = 44$ mS/cm², a change similar to the 10% increase in synaptic current in Fig. 4A). AP amplitude increased in both recording locations. However, because the amplitude of APs in the axon mainly depends on the sodium equilibrium potential and less so on the total current, AP amplitudes measured in the neurite changed only by few percent (Fig. 4E, i, ii).

To determine the combinatorial effect of a temperature-induced increase in the leak conductance in the neurite and so-dium conductance in the axon, both were increased simultaneously. The AP measured at both recording sites showed a decrease in amplitude relative to the baseline AP at each location. Figure 4D, i and ii, shows a sodium conductance increase of 10% and a leak conductance increase of 30% (compare blue and purple traces). The distance of the recording sites from the signal

origin thus appeared to matter less than for ePSPs. In fact, we found that about the same number of parameter combinations led to a decrease of AP amplitude at both locations (500 μ m and 1250 μ m; Fig. 4*E*, i, ii, squares below the solid black line). This suggests that the AP amplitude will largely reflect changes in membrane shunt, no matter where one records in the neurite. Figure 4*F* schematizes this conclusion. Specifically, unless APs are measured very close to the AP origin (red area, left of graph) or there is very little change in the membrane shunt, AP amplitude will decrease at warmer temperatures.

Our model suggests that temperature has distinct actions on ePSP and AP amplitude. Postsynaptic potential amplitude increases with synaptic current levels and is less likely to reflect shunt when recorded close to the ePSP initiation site. However, because of the increased membrane shunt, amplitude quickly diminishes over distance and signal invasion into distant regions of the neurite is diminished (Fig. 4C). On the other hand, when APs passively propagate through a neurite, amplitude primarily diminishes when shunt increases, even if other active conductances increase because these have only a small effect on the AP amplitude before entering the neurite (Fig. 4F). These results thus indicate that changes in our electrophysiological recordings of ePSP amplitude likely reflect the temperature-induced increase in synaptic current from 10 to 13°C more than they reflect the increase in membrane shunt. On the other hand, changes in AP amplitude reflect primarily the change in membrane shunt.

Neuropeptide modulation decreases membrane shunt

Our experimental data demonstrate that CabTRP Ia modulation increases electrical spread in the LG neurite. The underlying hypothesis is that CabTRP Ia counterbalances membrane shunt through the voltage-current relationship of the ionic current it activates. CabTRP Ia activates a well-characterized voltage-gated cation conductance (I_{MI}, modulator-induced current; Swensen and Marder, 2001). I_{MI} has an inverted bell-shaped voltage-current relationship (Zhao et al., 2010) and has been suggested to act as a negative leak conductance because of the linear falling edge of its voltage-current relationship (Bose et al., 2014). A negative leak conductance should effectively counterbalance leak and thus membrane shunt. We tested whether the effective membrane shunt, measured as the reciprocal of the total resistance across the membrane, was altered by CabTRP Ia. Membrane resistance was measured in a two-electrode voltage clamp (see above, Materials and Methods).

In saline, membrane resistance decreased significantly when temperature was increased from 10 to 13°C (Fig. 5A, one-way rmANOVA, $F_{(5,3)} = 20.696$, p < 0.001; Student–Newman–Keuls method pairwise comparisons, 10°C saline to 13°C saline, p <0.05). This supports our prediction that shunt increases with higher temperatures and is consistent with the previous literature (Städele et al., 2015). When CabTRP Ia was bath applied to the STG, membrane resistance increased at both temperatures when compared with the respective saline controls (Fig. 5A, 10°C saline to 10°C CabTRP Ia, p < 0.05, and 13°C saline to 13°C CabTRP Ia, p < 0.05). Membrane resistance at 10°C in CabTRP Ia was higher than at 13°C in CabTRP Ia (Fig. 5A, 10°C CabTRP Ia to 13°C CabTRP Ia, p < 0.05), indicating that temperature still altered membrane shunt when the CabTRP Ia was present. In summary, CabTRP Ia modulation increased resistance, which is consistent with the prediction that it counterbalances the temperature-induced shunt and increases dendritic electrical signal spread in LG.

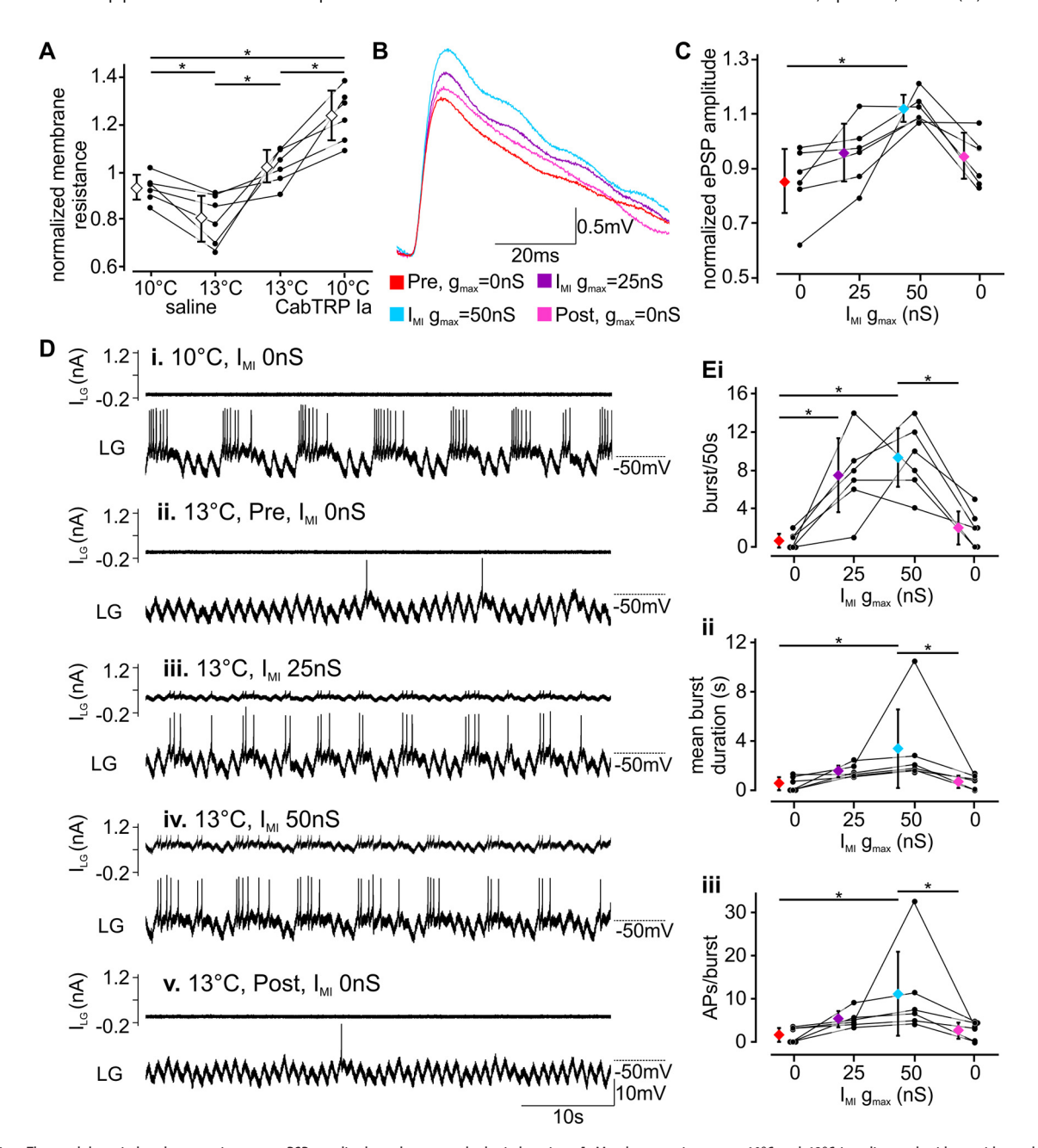


Figure 5. The modulator-induced current increases ePSP amplitude and restores rhythmic bursting. A, Membrane resistance at 10° C in saline and with peptide modulation by CabTRP Ia, normalized to the average value for each animal (N = 6). B, Average traces of ePSPs (n = 20/trace) measured from the LG soma when I_{MI} was artificially introduced using dynamic clamp. C, Across animals (N = 6), ePSP amplitude significantly increased from baseline at 50 nS of injected I_{MI} conductance. Paired data are connected with lines. D, Intracellular recordings of LG activity during 10 Hz MCN1 stimulation elicited a gastric mill rhythm at 10° C (i). LG spiking was absent at 13° C (ii). I_{MI} activation at 13° C restored LG spiking with 25 nS (iii) and more consistent bursts at 50 nS (iv). Removal of I_{MI} again silenced LG (v). E, Quantification of the number of (i) bursts/50 s, (ii) mean burst duration, and (iii) number of APs/burst before, during, and after I_{MI} activation. In one animal, 50 nS I_{MI} injection led to nearly tonic spiking in LG indicative of overexcitation leading to long burst durations and a larger number of APs per burst. *p < 0.05.

$I_{\rm MI}$ Activation is sufficient to restore electrical spread and rhythmic bursting at elevated temperatures

The actions of CabTRP Ia on LG appear to be exclusively mediated by the ionic current it activates, $I_{\rm MI}$ (DeLong et al., 2009a). Thus, we predicted that $I_{\rm MI}$ is sufficient to restore dendritic electrical spread in LG at higher temperatures. To test this prediction, we used dynamic clamp to inject $I_{\rm MI}$ into LG while we measured ePSP amplitude from the soma at 13°C, at constant membrane potentials. The dynamic clamp used previously published parameters for $I_{\rm MI}$ (DeLong et al., 2009b; Städele et al., 2015; see above, Materials and Methods). We used a two-

electrode setup, where membrane potential measurement and current injections were conducted through separate electrodes. $I_{\rm MI}$ was calculated in real time. Two maximum conductance levels were used, 50 nS and 25 nS, which corresponded to the conductance level previously published (Swensen and Marder, 2000; DeLong et al., 2009b), and half of that level.

We found that adding I_{MI} to LG at 13°C tended to increase ePSP amplitude. Figure 5*B* shows averaged ePSPs (n = 20 ePSPs/trace) at 0 nS, 25 nS, 50 ns, and at a 0 nS post-control (red, purple, blue, pink traces respectively). Injection of 50 nS showed the largest increase (compare red and blue

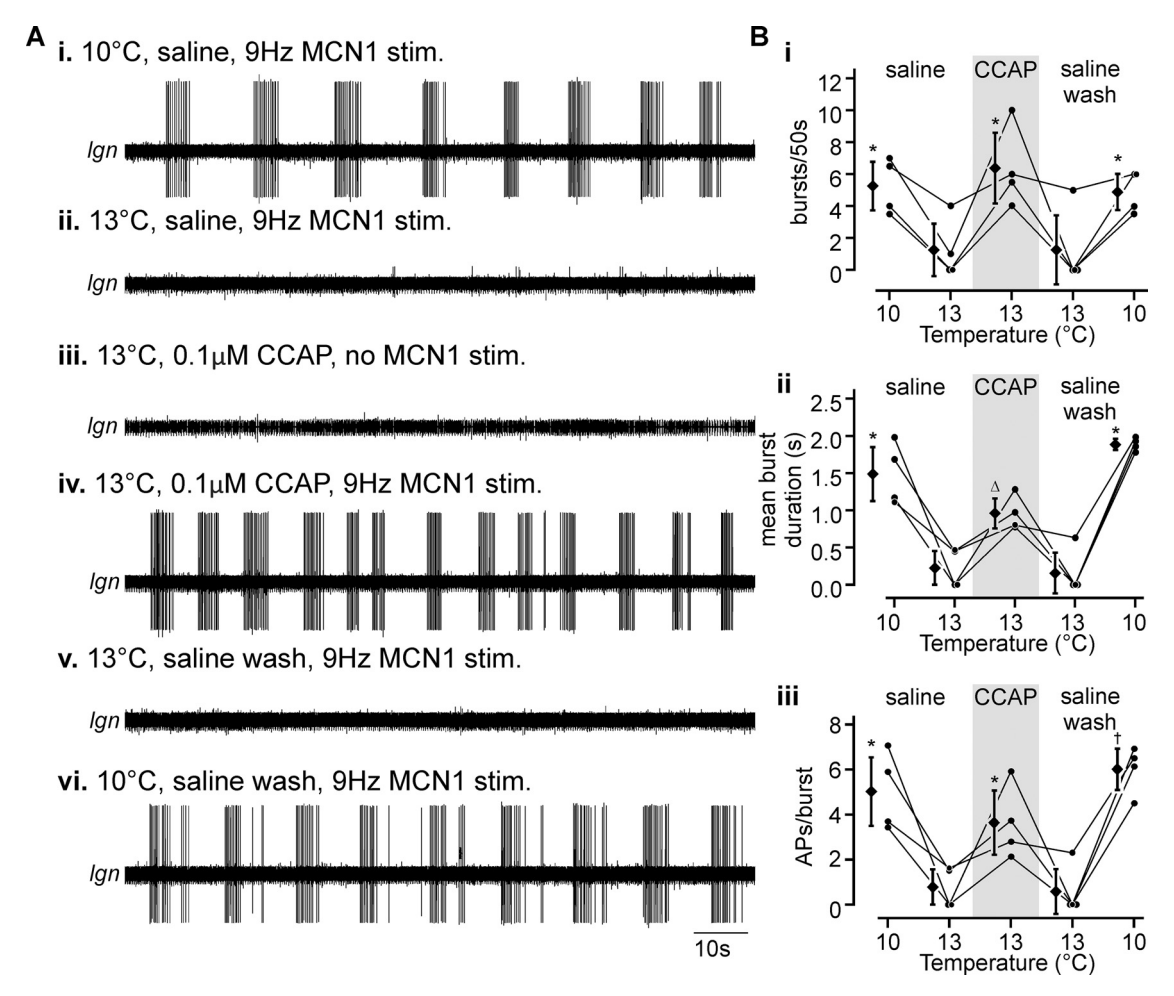


Figure 6. CCAP restores gastric mill rhythms after a crash at 13°C. A, Representative extracellular recording of LG activity on the lgn. A gastric mill rhythm was elicited at 10°C with 9 Hz tonic stimulation of MCN1 (i). MCN1 stimulation at the same frequency failed to elicit a gastric mill rhythm at 13°C (ii). In the absence of MCN1 stimulation, 0.1 μ M CCAP did not cause LG spiking and did not restore the gastric mill rhythm at 13°C (iii). Stimulating MCN1, however, in the presence of CCAP did restore LG spiking and the gastric mill rhythm (iv). In saline wash, MCN1 stimulation again failed to elicit a gastric mill rhythm at 13°C (v), but reducing the temperature back to 10°C restored the gastric mill rhythm (vi). B, Quantification of the number of bursts/50 s (i), mean burst duration (ii), and number of APs/burst (iii) at 10°C and 13°C in Saline, 13°C in CCAP, and 13°C in saline following a washout of CCAP. *significant difference (p < 0.05) from 13°C saline wash. Δ significant difference (p < 0.05) from all other conditions. †significant difference (p < 0.05) from 13°C saline wash, and 13°C CCAP.

traces), and this increase was significant across animals (Fig. 5C; one-way rmANOVA $F_{(5,3)}=5.303$, p=0.011, Holm–Sidak multiple comparisons, before 0 nS $I_{\rm MI}$ vs 50 nS $I_{\rm MI}$, p<0.05). These data thus demonstrate that $I_{\rm MI}$ indeed acts to counterbalance the temperature-induced shunt in the LG neuropil.

In fact, $I_{\rm MI}$ was also sufficient to rescue the gastric mill from a temperature-induced crash. We elicited a gastric mill rhythm at 10°C by increasing MCN1 stimulation frequency (Fig. 5D, i). We then increased the temperature to 13°C, which terminated the rhythm (Fig. 5D, ii). We then used the dynamic clamp to add 25 nS or 50 nS of $I_{\rm MI}$ at 13°C. Both conductance levels enabled LG to produce APs at 13°C. With 25 nS, LG activity was irregular and showed bursts of greatly varying durations (Fig. 5D, iii). At 50 nS, the conductance level previously published to be present in LG during gastric mill rhythms (DeLong et al., 2009b), LG bursting became regular (Fig. 5D, iv). These influences were reversible as removing I_{MI} led to an immediate cessation of the rhythm (Fig. 5D, v). Across animals, we found that the number of bursts (Fig. 5E, i, one-way rmANOVA, $F_{(5,3)} = 12.430$, p <0.001; Student-Newman-Keuls method pairwise comparisons, before 0 nS I_{MI} vs 50 nS, p < 0.05; after 0 nS I_{MI} vs 50 nS I_{MI} , p < 0.05), mean burst duration (Fig. 5E, ii, Friedman rmANOVA $Chi^2 = 15.103$, df = 3, p = 0.002; Tukey's post hoc test, before 0 nS

 $I_{\rm MI}$ vs 50 nS, p<0.05; after 0 nS $I_{\rm MI}$ vs 50 nS $I_{\rm MI}$, p<0.05), and number of spikes per burst increased significantly with 50 nS of $I_{\rm MI}$ from that of either the precontrol or postcontrol (Fig. 5*E*, iii, Friedman rmANOVA, Chi² = 17.526, df = 3, p<0.001; Tukey's post hoc test, before 0 nS $I_{\rm MI}$ vs 50 nS, p<0.05; after 0 nS $I_{\rm MI}$ vs 50 nS $I_{\rm MI}$, p<0.05). This suggests that $I_{\rm MI}$ is sufficient to restore electrical spread in the LG neuropil and thereby restores the rhythmic bursting necessary for a gastric mill rhythm.

As a final test of whether activating $I_{\rm MI}$ was a generalizable mechanism to restore the gastric mill rhythm, we activated $I_{\rm MI}$ by bath applying CCAP, 0.1–0.5 μ M, to the STG. CCAP is not released by MCN1 but instead circulates as a hormone in the hemolymph (Skiebe, 2001). Additionally, CCAP activates $I_{\rm MI}$ (Swensen and Marder, 2000) through receptors distinct from those activated by CabTRP Ia (Marder and Bucher, 2007; Garcia et al., 2015). We repeated our general experimental design (Fig. 1) in which we stimulated MCN1 at frequencies high enough to establish a baseline gastric mill rhythm at 10°C in saline (Fig. 6A, i). Then, we increased the temperature to 13°C and repeated the same stimulation. Consistent with our previous results and published data (Städele et al., 2015), no gastric mill rhythm could be initiated (Fig. 6A, ii). However, bath applying CCAP (0.1 μ M) restored the gastric mill rhythm at 13°C. Specifically, the

presence of CCAP by itself did not elicit spike activity or bursting in LG (Fig. 6A, iii). However, when MCN1 was additionally stimulated at the same baseline frequency sufficient to elicit a gastric mill rhythm at 10°C but failed at 13°C, the rhythm could now be started (Fig. 6A, iv). This suggests that the additional activation of I_{MI} through CCAP restored the LG rhythmic spiking, enabling the gastric mill rhythm. Washing out CCAP returned LG to the previous state in which MCN1 stimulation failed to elicit a 13°C but was successful at 10°C (Fig. 6A, v, vi). These effects were consistent across several animals (N = 4). Figure 6B, i-iii, compares the bursting activity of LG at 10°C and 13°C in saline and CCAP when MCN1 was stimulated at a frequency that elicited a gastric mill rhythm at 10°C in saline. We found that across preparations, the number of bursts per 50 s burst duration and spikes per burst were significantly larger at 13°C in the presence of CCAP than in saline before CCAP application or saline wash after CCAP application at the same temperature (Fig. 6B, i, bursts per 50 s, one-way rmANOVA, $F_{(4,3)}$ = 10.848, p < 0.001; Student-Newman-Keuls method pairwise comparisons, 13°C CCAP to 13°C saline, p < 0.05; 13°C CCAP to 13°C saline wash, p < 0.05; Fig. 6B, ii, burst duration, one-way rmANOVA, $F_{(4,3)} = 27.154$, p < 0.001; Student–Newman–Keuls method pairwise comparisons, 13°C CCAP to 13°C saline, p <0.05; 13°C CCAP to 13°C saline wash, p < 0.05; Fig. 6B, iii, number of spikes per burst, one-way rmANOVA $F_{(4,3)} = 16.582$, p <0.001; Student-Newman-Keuls method pairwise comparisons, 13°C CCAP to 13°C saline, p < 0.05; 13°C CCAP to 13°C saline wash, p < 0.05). Additionally, at 13°C in CCAP neither the number of bursts per 50 s nor the number of spikes per burst were significantly different from 10°C in saline (bursts per 50 s, 13°C CCAP to 10°C saline, n.s.; 13°C CCAP to 10°C saline wash, n.s.; spikes per burst, 13°C CCAP to 10°C saline, n.s.; 13°C CCAP to 10°C saline wash, n.s.). These results suggest that CCAP is sufficient to restore the gastric mill rhythm at elevated temperatures. Overall, our data suggest that activation of I_{MI} is a general mechanism that increases electrical spread in neurons to strengthen the temperature robustness of rhythmic pattern generators.

Discussion

Our results show that high temperatures shunt the neuronal membrane and lead to a reduction of passive propagation within the LG neuropil. This temperature-induced reduction is counterbalanced by neuropeptide modulation, which extends the dendritic electrical spread and rescues LG activity.

Temperature responses of crustacean stomatogastric neurons are well characterized, especially with respect to the remarkably robust and constitutively active pyloric rhythm (Tang et al., 2010, 2012). It maintains stereotypic activity independently of extrinsic inputs even when temperature increases by >15°C. Computational models have suggested that homeostatic processes via the coordinated temperature dependencies of opposing ion channels (e.g., IA vs Ih) or channel gates (activation vs inactivation gates) at AP initiation sites or in axons underlie this robustness (Tang et al., 2010; DeMaegd and Stein, 2020). Indeed, coordinated ion channel expression has been described for STG neurons (Golowasch et al., 1999; Khorkova and Golowasch, 2007) and others (Linsdell and Moody, 1994; Desai et al., 1999) as a mechanism for homeostatic plasticity. This may be particularly true for constitutively active circuits with stereotypical output, such as CPGs driven by endogenous pacemakers, where homeostatic processes continuously regulate activity.

Here, we describe a complimentary mechanism for temperature compensation whereby neuromodulation, rather than intrinsic coordination, enables temperature-robust activity. Alone, LG is not intrinsically temperature compensated and fails to elicit bursts fundamental to the gastric mill rhythm after a warming of only 3°C. Differential activation of descending projection neurons varies LG activity over time and in different sensory conditions (Hedrich et al., 2009; Yarger and Stein, 2015). This leads to the gastric mill rhythm being episodic and dependent on food presence, which reduces the feasibility of continuous homeostatic control of intrinsic properties. A more flexible compensation mechanism for acute temperature changes may thus be required in episodic CPGs.

LG activity relies on the propagation and summation of synaptic input from descending projection neurons and its half-center partner (Stein et al., 2007). However, we observed that summation of synaptic inputs is not intrinsically temperature robust because at elevated temperatures the distance individual ePSPs traveled was diminished. This was concurrent with an increase in membrane shunt and spike failure. CabTRP Ia modulation reversed these effects, indicating that membrane shunt was counterbalanced by the actions of the neuropeptide, increasing the length constant within the neuropil. Indeed, our recordings show that I_{MI}, the inward current elicited by CabTRP Ia or CCAP, was sufficient to increase dendritic electrical spread and restore LG bursts. Thus, although it may be imperative for continuously active neurons and circuits to prepare for the entire range of temperatures an animal may experience, a more flexible method of compensation may better suit episodically active neurons and circuits.

Membrane shunt diminishes passive propagation and hyperpolarization reduces synaptic current input

Our optical and electrical data are consistent with elevated temperatures diminishing dendritic electrical spread and CabTRP Ia modulation increasing it. The ePSP amplitudes measured in the soma, however, although increased by CabTRP Ia, appeared to be unaffected by temperature changes (Fig. 3C). This was unexpected and contrary to previous studies showing that ePSP amplitude decreases with temperature (Städele et al., 2015). However, in our study we prevented the LG resting membrane potential from hyperpolarizing as the temperature increased. This removed voltage-dependent changes in the MCN1-LG electrical synapse that reduce ePSP amplitude but uncovered a temperature-dependent increase in synaptic current. This led to questions about the extent to which membrane shunt versus synaptic input levels affect our measurements. Our model indicates that at short electrotonic distances between synaptic input and recording site, synaptic current dominates the response, and ePSP amplitudes can increase even with greater membrane shunt (Fig. 4C). In contrast, at longer electrotonic distances, membrane shunt dominates the response and ePSP amplitudes decrease.

We do not know the electrotonic distances between MCN1 synapses, the LG soma where we recorded ePSPs, and the LG spike initiation site critical for spike generation. Measurements of length constants in other STG neurons indicate that neuropils are electrotonically compact with length constants of $>1000~\mu m$. STG neuropil anatomy also seems to support the propagation of synaptic signals because of continuously decreasing axial resistance from small tertiary neurites to the larger primary neurites (Otopalik et al., 2019). However, STG neuron spike initiation sites are

spatially distant from the neuropil, close to where the main motor nerve exits the ganglion (Miller and Selverston, 1979; Raper, 1979). The main neurites projecting toward the motor nerve show no consistent diameter changes (DeMaegd and Stein, 2020), suggesting that synaptic signal amplitude will diminish toward the spike initiation sites, and membrane shunt will dominate PSP amplitude. This is consistent with our finding that at elevated temperatures, ePSPs penetration of the neuropil is reduced, and MCN1 stimulation is insufficient to consistently elicit action potentials.

Although membrane shunt is likely the dominant factor restricting synaptic signals from reaching the spike initiation site, the hyperpolarization-induced reduction of input from the MCN1-LG electrical synapse may additionally reduce ePSP amplitude. The voltage dependence of the electrical synapse opposes the temperature-induced increase in synaptic current, which would explain why ePSP amplitudes have previously been reported to diminish at warmer temperatures (Städele et al., 2015). If hyperpolarization of LG was the major contributor to burst failure, the gastric mill rhythm should recover if the resting membrane potential is depolarized to the level at lower temperatures. Städele et al. (2015) did this experiment and found that although APs were more likely to be elicited, the characteristic bursts of the gastric mill rhythm were absent, suggesting that synaptic summation was incomplete. In contrast, counterbalancing leak (Städele et al., 2015), applying CabTRP Ia (Fig. 1C) or CCAP (Fig. 6A), or adding I_{MI} (Fig. 5D) restored rhythmic bursts, further suggesting that decreasing membrane shunt is critical to restore proper bursting. Thus, although altering the resting membrane potential of LG is influential, counterbalancing shunt restores its rhythmic activity.

Furthermore, our calcium imaging with variable resting membrane potential and the somatic AP amplitude measurements with constant membrane potential indicated that AP invasion in the neuropil decreased at 13°C. Because of the total amplitude of ~100 mV (Bucher et al., 2003), AP amplitudes are more resistant to temperature-induced membrane hyperpolarization. Once APs antidromically enter the passive LG neurites, membrane shunt affects them similar to all other passive signals, making them ideal for measuring electrical spread. Antidromic APs passively backpropagate into the neuropil of STG but have only limited effects on pattern generation (Mulloney and Selverston, 1972; Meyrand et al., 1992), presumably because APs do not penetrate fine neuropilar structures. Our imaging data corroborates this assumption. The morphology of the STG neuropil (Otopalik et al., 2019), although advantageous for orthodromic electrical signals, antagonizes antidromic propagation because of increasingly larger axial resistances resulting from smaller diameter neurites. At 10°C, much of the calcium signal was obtained in the main neurite and was less prevalent at 13°C. In CabTRP Ia, however, AP penetration of the neuropil was much larger at both temperatures, further supporting that neuropeptide modulation increased electrical spread in LG.

How does CabTRP Ia increase electrical spread?

Membrane shunt is often associated with increases in leak currents. Changes in leak currents have long been known to play important roles in the regulation of excitability (Rekling et al., 2000; Brickley et al., 2007), switches in activity states of neurons (Gramoll et al., 1994), and the control of network oscillations (Cymbalyuk et al., 2002; Blethyn et al., 2006; Koizumi et al., 2008; Zhao et al., 2010). The modulation of leak currents by neurotransmitters has been proposed to contribute to the regulation

of neuronal excitability (Aller et al., 2005; Kim, 2005; Pratt and Aizenman, 2007), but few studies have provided functional context for such modulation or its effects on signal processing in neurons. This study provides direct evidence that neuropeptide modulation increases electrical spread by activating an inward current that counterbalances membrane shunt. I_{MI} is a second messenger-activated voltage-dependent inward current similar to that evoked by NMDA channels (Swensen and Marder, 2000). The negative slope in a portion of its inverted bell-shaped current-voltage relationship acts as a negative leak conductance (Zhao et al., 2010), increasing excitability when artificially injected into neurons (DeLong et al., 2009b). Previous model studies also suggest it acts to counterbalance temperatureinduced increases in leak in the LG neuron (Städele et al., 2015). Our application of CabTRP Ia, CCAP, and a dynamic clamp protocol demonstrate that I_{MI} also promotes dendritic electrical spread, enabling the propagation of synaptic inputs and restoring rhythmicity of LG at elevated temperatures.

Peptide modulation as a general mechanism for rhythmic stability

Neuropeptides have been implicated in modulating many pattern generating networks, including some in the mammalian CNS, although the cellular actions are far from understood (Mutolo et al., 2010). For example, substance P has been shown to increase excitability necessary for pattern generation in the rodent pre-Bötzinger complex (Gray et al., 1999). Additionally, reduced peptide and peptide receptor expression has been associated with a number of respiratory diseases that are further exacerbated when respiratory tissues are exposed to temperature changes (Filiano and Kinney, 1994). For instance, abnormal PACAP (pituitary adenylate cyclase-activating polypeptide) and its receptor Pac1 expression has been observed in postmortem human sudden infant death syndrome infant brainstems (Huang et al., 2017; Shi et al., 2021), and deletion of *Pac1* expression in neonatal mice pre-Bötzinger complex reduces ventilatory responsiveness to changes in CO2 or hypoxia (Shi et al., 2021). The mechanisms by which these factors interact and affect the respiratory networks, however, are unclear. Our data show that substance-P-related modulation enhances gastric mill network robustness by increasing dendritic electrical spread. Neuromodulation allowed for fast, transient, and specific regulation of the temperature sensitivity, quickly adjusting the permissive temperature range of the system. Although this mechanism may be better suited for episodic networks or those that generate highly variable patterns, the abundance of neuropeptides in most pattern generating networks and the clear impact of shunt to neuronal processing lend support that we have identified a general mechanism for sustaining neuronal activity.

References

Aller MI, Veale EL, Linden AM, Sandu C, Schwaninger M, Evans LJ, Korpi ER, Mathie A, Wisden W, Brickley SG (2005) Modifying the subunit composition of TASK channels alters the modulation of a leak conductance in cerebellar granule neurons. J Neurosci 25:11455–11467.

Ballo AW, Nadim F, Bucher D (2012) Dopamine modulation of Ih improves temporal fidelity of spike propagation in an unmyelinated axon. J Neurosci 32:5106–5119.

Bartos M, Manor Y, Nadim F, Marder E, Nusbaum MP (1999) Coordination of fast and slow rhythmic neuronal circuits. J Neurosci 19:6650–6660.

- Blethyn KL, Hughes SW, Toth TI, Cope DW, Crunelli V (2006) Neuronal basis of the slow (<1 Hz) oscillation in neurons of the nucleus reticularis thalami in vitro. J Neurosci 26:2474–2486.
- Bose A, Golowasch J, Guan Y, Nadim F (2014) The role of linear and voltage-dependent ionic currents in the generation of slow wave oscillations. J Comput Neurosci 37:229–242.
- Brickley SG, Aller MI, Sandu C, Veale EL, Alder FG, Sambi H, Mathie A, Wisden W (2007) TASK-3 two-pore domain potassium channels enable sustained high-frequency firing in cerebellar granule neurons. J Neurosci 27:9329–9340.
- Bucher D, Thirumalai V, Marder E (2003) Axonal dopamine receptors activate peripheral spike initiation in a stomatogastric motor neuron. J Neurosci 23:6866–6875.
- Cao XJ, Oertel D (2005) Temperature affects voltage-sensitive conductances differentially in octopus cells of the mammalian cochlear nucleus. J Neurophysiol 94:821–832.
- Coleman MJ, Meyrand P, Nusbaum MP (1995) A switch between two modes of synaptic transmission mediated by presynaptic inhibition. Nature 378:502–505.
- Collins CA, Rojas E (1982) Temperature dependence of the sodium channel gating kinetics in the node of Ranvier. Q J Exp Physiol 67:41–55.
- Cymbalyuk GS, Quentin G, Masino MA, Calabrese RL (2002) Bursting in leech heart interneurons: cell autonomous and network based mechanisms. J Neurosci 22:10580–10592.
- DeLong ND, Beenhakker MP, Nusbaum MP (2009a) Presynaptic inhibition selectively weakens peptidergic cotransmission in a small motor system. J Neurophysiol 102:3492–3504.
- DeLong ND, Kirby MS, Blitz DM, Nusbaum MP (2009b) Parallel regulation of a modulator-activated current via distinct dynamics underlies comodulation of motor circuit output. J Neurosci 29:12355–12367.
- DeMaegd ML, Stein W (2020) Temperature-robust activity patterns arise from coordinated axonal sodium channel properties. PLoS Comput Biol 16:e1008057.
- DeMaegd ML, Städele C, Stein W (2017) Axonal conduction velocity measurement. Bio-Protocol 7:e2152.
- Desai NS, Rutherford LC, Turrigiano GG (1999) Plasticity in the intrinsic excitability of cortical pyramidal neurons. Nat Neurosci 2:515–520.
- Filiano JJ, Kinney HC (1994) A perspective on neuropathologic findings in victims of the sudden infant death syndrome: the triple-risk model. Biol Neonate 65:194–197.
- Fleming PJ, Azaz Y, Wigfield R (1992) Development of thermoregulation in infancy: possible implications for SIDS. J Clin Pathol 45:17–19.
- Garcia VJ, Daur N, Temporal S, Schulz DJ, Bucher D (2015) Neuropeptide receptor transcript expression levels and magnitude of ionic current responses show cell type-specific differences in a small motor circuit. J Neurosci 35:6786–6800.
- Golowasch J, Abbott LF, Marder E (1999) Activity-dependent regulation of potassium currents in an identified neuron of the stomatogastric ganglion of the crab *Cancer borealis*. J Neurosci 19:RC33–RC33.
- Gramoll S, Schmidt J, Calabrese RL (1994) Switching in the activity state of an interneuron that controls coordination of the hearts in the medicinal leech (*Hirudo medicinalis*). J Exp Biol 186:157–171.
- Gray PA, Rekling JC, Bocchiaro CM, Feldman JL (1999) Modulation of respiratory frequency by peptidergic input to rhythmogenic neurons in the preBötzinger complex. Science 286:1566–1568.
- Gutierrez GJ, Grashow RG (2009) Cancer borealis stomatogastric nervous system dissection. J Vis Exp 25:e1207.
- Hedrich UB, Smarandache CR, Stein W (2009) Differential activation of projection neurons by two sensory pathways contributes to motor pattern selection. J Neurophysiol 102:2866–2879.
- Hedrich UB, Diehl F, Stein W (2011) Gastric and pyloric motor pattern control by a modulatory projection neuron in the intact crab *Cancer pagurus*. J Neurophysiol 105:1671–1680.
- Heitler WJ, Edwards DH (1998) Effect of temperature on a voltage-sensitive electrical synapse in crayfish. J Exp Biol 201:503–513.
- Hille B (2001) Ionic channels of excitable membranes. Sunderland, MA:
- Hines ML, Carnevale NT (2001) NEURON: a tool for neuroscientists. Neuroscientist 7:123–135.
- Hodgkin A, Huxley A (1952a) Currents carried by sodium and potassium ions through the membrane of the giant axon of Loligo. J Physiol 116:449-472.

- Hodgkin AL, Huxley AF (1952b) A quantitative description of membrane current and its application to conduction and excitation in nerve. J Physiol 117:500–544.
- Hoffman DA, Magee JC, Colbert CM, Johnston D (1997) K+ channel regulation of signal propagation in dendrites of hippocampal pyramidal neurons. Nature 387:869–875.
- Huang J, Waters KA, Machaalani R (2017) Pituitary adenylate cyclase activating polypeptide (PACAP) and its receptor 1 (PAC1) in the human infant brain and changes in the sudden infant death syndrome (SIDS). Neurobiol Dis 103:70–77.
- Khorkova O, Golowasch J (2007) Neuromodulators, not activity, control coordinated expression of ionic currents. J Neurosci 27:8709–8718.
- Kim D (2005) Physiology and pharmacology of two-pore domain potassium channels. Curr Pharm Des 11:2717–2736.
- Koizumi H, Wilson CG, Wong S, Yamanishi T, Koshiya N, Smith JC (2008) Functional imaging, spatial reconstruction, and biophysical analysis of a respiratory motor circuit isolated in vitro. J Neurosci 28:2353–2365.
- Linsdell P, Moody WJ (1994) Na+ channel mis-expression accelerates K+ channel development in embryonic *Xenopus laevis* skeletal muscle. J Physiol 480 (Pt 3)::405–410.
- Marder E, Bucher D (2007) Understanding circuit dynamics using the stomatogastric nervous system of lobsters and crabs. Annu Rev Physiol 69:291–316.
- Meyrand P, Weimann JM, Marder E (1992) Multiple axonal spike initiation zones in a motor neuron: serotonin activation. J Neurosci 12:2803–2812.
- Miller JP, Selverston A (1979) Rapid killing of single neurons by irradiation of intracellularly injected dye. Science 206:702–704.
- Mulloney B, Selverston A (1972) Antidromic action potentials fail to demonstrate known interactions between neurons. Science 177:69–72.
- Mutolo D, Bongianni F, Cinelli E, Pantaleo T (2010) Role of neurokinin receptors and ionic mechanisms within the respiratory network of the lamprey. Neuroscience 169:1136–1149.
- Nadim F, Manor Y, Nusbaum MP, Marder E (1998) Frequency regulation of a slow rhythm by a fast periodic input. J Neurosci 18:5053–5067.
- Norris BJ, Coleman MJ, Nusbaum MP (1996) Pyloric motor pattern modification by a newly identified projection neuron in the crab stomatogastric nervous system. J Neurophysiol 75:97–108.
- Otopalik AG, Sutton AC, Banghart MR, Marder E (2017) When complex neuronal structures may not matter. eLife 6:e23508.
- Otopalik AG, Pipkin J, Marder E (2019) Neuronal morphologies built for reliable physiology in a rhythmic motor circuit. eLife 8:e41728.
- Pratt KG, Aizenman CD (2007) Homeostatic regulation of intrinsic excitability and synaptic transmission in a developing visual circuit. J Neurosci 27:8268–8277.
- Raper JA (1979) Nonimpulse-mediated synaptic transmission during the generation of a cyclic motor program. Science 205:304–306.
- Rekling JC, Funk GD, Bayliss DA, Dong XW, Feldman JL (2000) Synaptic control of motoneuronal excitability. Physiol Rev 80:767–852.
- Robertson RM, Money TG (2012) Temperature and neuronal circuit function: compensation, tuning and tolerance. Curr Opin Neurobiol 22:724– 734
- Schindelin J, Arganda-Carreras I, Frise E, Kaynig V, Longair M, Pietzsch T, Preibisch S, Rueden C, Saalfeld S, Schmid B, Tinevez J-Y, White DJ, Hartenstein V, Eliceiri K, Tomancak P, Cardona A (2012) Fiji: an opensource platform for biological-image analysis. Nat Methods 9:676–682.
- Sharp AA, O'Neil MB, Abbott LF, Marder E (1993) Dynamic clamp: computer-generated conductances in real neurons. J Neurophysiol 69:992–995.
- Shi Y, Stornetta DS, Reklow RJ, Sahu A, Wabara Y, Nguyen A, Li K, Zhang Y, Perez-Reyes E, Ross RA, Lowell BB, Stornetta RL, Funk GD, Guyenet PG, Bayliss DA (2021) A brainstem peptide system activated at birth protects postnatal breathing. Nature 589:426–430.
- Short SM, Oikonomou KD, Zhou W-L, Acker CD, Popovic MA, Zecevic D, Antic SD (2017) The stochastic nature of action potential backpropagation in apical tuft dendrites. J Neurophysiol 118:1394–1414.
- Skiebe P (2001) Neuropeptides are ubiquitous chemical mediators: using the stomatogastric nervous system as a model system. J Exp Biol 204:2035– 2048
- Städele C, Andras P, Stein W (2012) Simultaneous measurement of membrane potential changes in multiple pattern generating neurons using voltage sensitive dye imaging. J Neurosci Methods 203:78–88.

- Städele C, Heigele S, Stein W (2015) Neuromodulation to the rescue: compensation of temperature-induced breakdown of rhythmic motor patterns via extrinsic neuromodulatory input. PLoS Biol 13:e1002265.
- Städele C, DeMaegd ML, Stein W (2017) Extracellular axon stimulation. Bio-Protocol 7:e2151.
- Stein W, DeLong ND, Wood DE, Nusbaum MP (2007) Divergent co-transmitter actions underlie motor pattern activation by a modulatory projection neuron. Eur J Neurosci 26:1148–1165.
- Swensen AM, Marder E (2000) Multiple peptides converge to activate the same voltage-dependent current in a central pattern-generating circuit. J Neurosci 20:6752–6759.
- Swensen AM, Marder E (2001) Modulators with convergent cellular actions elicit distinct circuit outputs. J Neurosci 21:4050–4058.
- Tang LS, Goeritz ML, Caplan JS, Taylor AL, Fisek M, Marder E (2010) Precise temperature compensation of phase in a rhythmic motor pattern. PLoS Biol 8:e1000469.

- Tang LS, Taylor AL, Rinberg A, Marder E (2012) Robustness of a rhythmic circuit to short- and long-term temperature changes. J Neurosci 32:10075–10085.
- Tryba AK, Ramirez J-M (2004) Hyperthermia modulates respiratory pacemaker bursting properties. J Neurophysiol 92:2844–2852.
- Yarger AM, Stein W (2015) Sources and range of long-term variability of rhythmic motor patterns in vivo. J Exp Biol 218:3950–3961.
- Zhao S, Golowasch J, Nadim F (2010) Pacemaker neuron and network oscillations depend on a neuromodulator-regulated linear current. Front Behav Neurosci 4:21.
- Zhao S, Sheibanie AF, Oh M, Rabbah P, Nadim F (2011) Peptide neuromodulation of synaptic dynamics in an oscillatory network. J Neurosci 31:13991–14004.
- Zhu Y, de Castro L, Cooper RL (2018) Effect of temperature change on synaptic transmission at crayfish neuromuscular junctions. Biol Open 7: bio037820.